J Solid State Electrochem (2009) 13:1327–1337
DOI 10.1007/s10008-008-0674-4

ORIGINAL PAPER

# A zirconia-polyester glycol coating on differently pretreated AISI 316L stainless steel: corrosion behavior in chloride solution

**C. Martinez · M. Sancy · J. H. Zagal · F. M. Rabagliati · B. Tribollet · H. Torres · J. Pavez · A. Monsalve · M. A. Paez**

Received: 29 June 2008 / Revised: 4 September 2008 / Accepted: 6 September 2008 / Published online: 7 October 2008


**Abstract** The effect of zirconia and zirconia-polyester glycol hybrid coatings on the corrosion resistance of mechanically polished or anodized AISI 316 stainless steel (316L), was studied by potentiodynamic polarization and electrochemical impedance spectroscopy in 0.1 M NaCl and scanning electron microscope and atomic force microscopy examinations. The deposition of zirconia coatings was achieved by the sol–gel technique by immersing the samples in either the inorganic polymer or the organic–inorganic polymer mixture. From potentiodynamic and impedance measurements, the grade of protection is reduced with the exposure time to the electrolyte, which is mainly associated with lost of film adhesion and, consequently, detachment from the metal substrate. However, the uncoated anodized sample revealed an unexpected corrosion behavior; the anodic film formed during anodizing readily increased the corrosion resistance of the 316L stainless steel in 0.1 M NaCl, revealing a considerable reduction in the corrosion current density and an increase in the pitting potential.

**Keywords** Sol–gel · Organic–inorganic hybrid coating · Stainless steel

C. Martinez · M. Sancy · J. H. Zagal · J. Pavez · M. A. Paez (✉)
Departamento de Química de los Materiales,
Facultad de Química y Biología,
Universidad de Santiago de Chile,
Casilla 40, Correo 33,
Santiago, Chile
e-mail: mpaez@usach.cl

F. M. Rabagliati
Departamento de Ciencias del Ambiente,
Facultad de Química y Biología,
Universidad de Santiago de Chile,
Casilla 40, Correo 33,
Santiago, Chile

B. Tribollet
Laboratoire Interfaces et systèmes Electrochimiques, CNRS,
Université Pierre et Marie Curie-Paris6,
UPR15-LISE.4 place Jussieu,
Paris 75005, France

H. Torres
Facultad de Ingeniería, Departamento de Ingeniería Química,
Grupo de Corrosión Y Protección,
Sede de Investigaciones Universitarias,
Universidad de Antioquia,
Calle 62 # 52–59, Torre 2,
Medellín, Colombia

A. Monsalve
Departamento de Metalurgia, Facultad de Ingeniería,
Universidad de Santiago de Chile,
Santiago, Chile

## Introduction

Stainless steels are widely used in numerous structural and marine applications because of their physical characteristics such as stiffness, high strength, and comparative good corrosion resistance regarding other commercial alloys [1–2]. Although one of the main reasons of using stainless steels is their corrosion resistance, they do present localized corrosion in some environments such as chloride containing solutions [3, 4]. The most common method of protection in aggressive environment is surface passivation followed by a costing of paint. The traditional surface passivation treatment for steel is phosphating, which is a commercial process that produce stable coatings, with insoluble phosphate of iron (II), Zinc (II), manganese (II), nickel (II) cations, or more often mixtures of them, bonded to the

metal substrate. However, because phosphate films are formed at cathodic sites, the film is susceptible to developing pinholes, which gives rise to a rapid film degradation under corrosive conditions such as salt water contact [1–3].

In recent years, there has been an effort to develop alternative protection methods for stainless steel. Thus, in acid media, stainless steel can be successfully protected with polypyrrole based composite films containing hexacyanoferrate anions [4–7]. The formation of robust Prussian blue results in the stabilization of passive state of the steel. Such films exhibit promising properties in the protection of stainless steel against pitting corrosion in chloride containing acid medium.

Among the alternative protection method, the sol–gel approach has been investigated as a technique to form protective films on different metals [8–12], because it provides films which are highly adherent and chemically inert at temperatures near room temperature. The sol–gel method consists of simultaneous hydrolysis and condensation reactions that originate from alkoxide precursors, to form glassy polymer networks exhibiting a micro- or nanoporous structure. In comparison to other coating technologies, sol–gel synthesis of thin films offers several potential advantages. Prior to gelation, the sol is ideal for preparing thin films by common processes, including dipping, spinning, or spraying [13]. These application methods generally produce thin films of submicrometer thickness. Preparation of thicker films is possible through application of multiple layers [12] or by variation of the withdrawing or spinning speed in the case of dip and spin coating [13], respectively.

A wide variety of alkoxide precursor materials commercially available have been reported to form protective films on steel [8–12]. In spite of all the advantages of sol–gel processing, sol–gel coatings are highly porous with poor mechanical resistance. Usually annealing or sintering processes is required to get dense microstructure [13]. However, the high temperature treatment may result in cracking or delamination of sol–gel coatings because of the large mismatch of thermal coefficients and possible chemical reaction at the interface [14]. In addition, annealing or sintering processes limit industrial application of sol–gel coating for corrosion protection and also, its application on temperature sensitive substrates and devices.

One alternative method to avoid high temperature treatments and to improve the mechanical properties of sol–gel derived coating is to synthesize hybrid organic–inorganic material. The hybrid organic–inorganic materials used to protect metallic surfaces from corrosion are composed of intimately mixed polymer systems [15–16]. The inorganic components tend to impart durability, scratch resistance, and improved adhesion to the metal substrates, while the organic components contribute increased flexibility, density, and functional compatibility with organic polymer paint systems. Furthermore, the impregnation of open pores by the organic material may reduce coating porosity, providing a high barrier for species diffusion from the electrolyte to the metal substrate [15]. Sol–gel derived hybrid materials have been prepared over a continuous compositional range from almost completely inorganic to almost completely organic. These hybrid films have been used in a variety of applications as chemically tailored materials with improved thermal, mechanical, optical, and electrical properties [17].

The aim of this work is to evaluate the effect of incorporating polyether glycol in sol–gel $ZrO_2$ coatings on the aqueous corrosion resistance of a stainless steel in a chloride solution. In addition, the influence of anodizing as a pretreatment to improve both film adhesion and corrosion resistance of the coated stainless steel is also investigated.

## Experimental

### Sample preparation

The substrate, 316L stainless steel, was provided as sheets of 1 mm in thickness of composition (wt.%): 67.25 Fe, 18.55 Cr, 11.16 Ni, 2.01 Mo, 0.026 Cu, 0.15 Si, and 0.028 C. The samples to be modified by the films were initially prepared in accordance with the following general sequences A or B: A—mechanical polished on 1200 and 2400 grit paper and B—mechanical polished on 1200 and 2400 grit paper followed by anodizing at a constant voltage of 12 V in 10% phosphoric acid for 30 min. The samples were then rinsed in distilled water and dried in a cold stream. After the previous surface treatment, the steel samples were immersed for 1 min in a 0.03 wt.% NaOH solution containing Triton X-100 as tensoactive, with constant stirring. The NaOH solution was used to hydrate the oxide film and the tensoactive to reduce the surface tension, both procedures to increase adhesion of the polymeric film.

Zirconium isopropoxide $Zr(OC_3H_7)4$ diluted in isopropanol ($C_3$,$H_7$,OH) was used as source of zirconia. The differently pretreated steel samples were dipped into a soaking bath of zirconium propoxide solution in the presence of nitric acid as catalyst at room temperature and kept there for 1 min and then withdrawn slowly. After dipping in the zirconium containing solution, the samples were cured at 60 °C for 30 min. A smooth and transparent layer, covering the metal surface, was visually observed. The hybrid polymer was prepared by mixing the inorganic and organic polymers, using polyether glycol (terathane 2000) as the organic component, in a molar ratio of 0.95:0.05, stirring thoroughly to allow a complete homogenization of the mixture.

### Film morphology

The steel surfaces were examined and analyzed in a JEOL 5410 scanning electron microscope (SEM) with energy dispersive X-ray (EDX) facilities and also examined by atomic force microscopy (AFM). The AFM surface analysis was done in a Nanoscope IIIa Extended Multimode AFM, Digital Instruments (Santa Barbara, CA, USA) with a "J" scanner. The surfaces were scanned in the Tapping$^{R}$ mode with a scan rate of 0.3 Hz, using commercially etched silicon probes (Digital Instruments) with a triangular tip.

### Electrochemical test

To elucidate the protective characteristic of the polymeric films, the open circuit potentials (OCP) of the coated and uncoated steel specimens were recorded for 70 h in 0.1 M NaCl. The corrosion resistance was evaluated by potentiodynamic polarization experiments in aerated 0.1 M NaCl solution, using a standard three electrode cell, steel-working electrode, Pt-counter electrode, and a standard $Hg/Hg_2SO_4$ reference electrode (SSE). Prior to testing, the steel electrodes were masked with one coat of Araldite to leave an exposed surface area of about 1 $cm^2$. The measurements were performed at room temperature, after the open circuit potential was stabilized to 3 mV for 5 min. The potential was scanned 800 mV in both anodic and cathodic directions, starting from the corresponding OCP. The potential scan rate was 0.1 mV $s^{-1}$. Electrochemical impedance spectroscopy was performed, sweeping frequencies from 500,000 to 0.01 Hz and modulating 0.01 V (rms) after an immersion time of 5 h.

## Results and discussion

### SEM examinations

Figure 1 shows scanning electron micrographs of the mechanical polished steel samples, with and without (Fig. 1a) zirconia-based sol–gel (Fig. 1b, c) and hybrid films (Fig. 1d). In general, the mechanical polished sample (Fig. 1a) reveals a relatively uniform morphology, with some scratched areas and a textured light appearance associated with local composition and second phase material. From EDX analysis, the composition of the metal is in good agreement with the general composition of AISI 316 stainless steel. In the case of sol–gel-coated steel samples (Fig. 1b, c), a terrace-like appearance is observed. The terrace areas, which are larger for the double-coated steel sample, are the result of shrinkage cracking associated with drying. This is possibly enhanced by weak film adhesion at surface regions related to second phases or local surface region of different compositions with respect to the matrix. This is confirmed by the zirconium and iron profile obtained by EDX analysis of coated surfaces. From the region labeled X to surface region between terraces, a progressive decrease in the zirconium content and a sudden increase in the iron content were determined. In contrast, the sample coated by the hybrid film reveals a very uniform surface, showing only the on-purpose scratched region of lighter appearance with respect to the general surface.

Figure 2 illustrates the SEM micrographs of the uncoated and coated anodized steel samples. For the uncoated sample, grain boundaries are evident, revealing grains of different sizes. This morphology is possibly the result of preferential oxide formation during anodizing, which is expected to occur to a low extent above grain boundaries, due to high local alloying element contents associated with the presence of second phases. EDX analysis at the boundary regions revealed higher chromium and nickel content with respect to the matrix. From Fig. 2b, c, a terrace-like appearance associated with shrinkage cracking and similar to those in Fig. 1b, c is revealed. Also, the zirconium and iron profile (EDX analysis) are like those of the coated mechanical polished samples. They show a progressive decrease in the zirconium content and a sudden increase in the iron content for the probe position moving away from the region labeled X in Fig. 2b, c. The coated area in Fig. 2b, c seems to be of the same size of the grains in the anodized sample (Fig. 2a). It is apparent then that the local composition and morphology of grain boundaries limit adhesion of the film in these regions, making the film above these regions susceptible to cracking during drying. A second application of sol–gel shows no difference in the terrace area outlined by the film (Fig. 2c). Conversely, the hybrid-coated anodized steel sample surface, which is not shown here, generally revealed higher uniformity with respect to those coated by zirconia sol–gel film, showing a similar appearance to that in Fig. 1d.

The differences in surface morphology of the differently coated steel samples were further confirmed by AFM examinations (Fig. 3). While the sol–gel-coated steel samples in Fig. 3a, b are comparatively similar to those revealed by SEM (Figs. 1b and 2b), revealing a terrace-like appearance, the AFM image of the hybrid sol–gel-coated steel sample reveals a very uniform surface. Such a surface morphology was stable even after 2 weeks of exposure in the laboratory atmosphere. Measurements of the sol–gel film thickness obtained by SEM examination at deliberately scratched film regions determined average film thicknesses of 312 and 425 nm for the single- and double-coated steel samples, respectively. These values were independent on the surface treatment given to the steel sample.

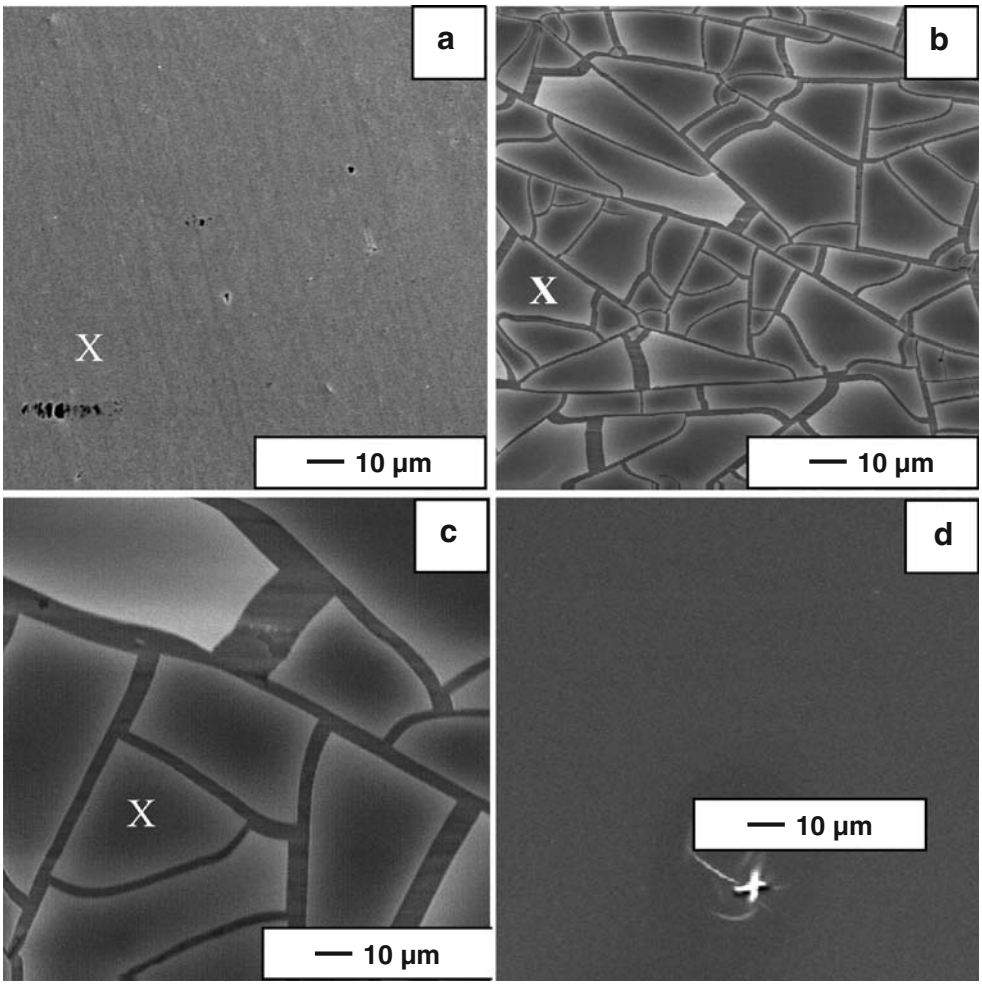


**Fig. 1** Scanning electron micrograph showing the surface morphology of uncoated and coated mechanical polished 316L stainless steel. **a** Uncoated sample, **b** zirconia single-coated sample, **c** zirconia double-coated sample, **d** hybrid sol–gel-coated steel surface

## Open circuit potential behavior

Figure 4a shows the OCP behavior of the uncoated and coated steel samples during 70 h. The OCP of the mechanical polished 316L steel samples shifted in the positive direction from the beginning of the test by about 300 mV, reaching a relatively constant value of about −0.3 V after 25 h. This is consistent with a $Fe/Fe^{+2}$ system evolving to the passivity region in the presence of chloride ions [1, 2], with passivation possibly due to oxide and hydroxide chromium formation. In general, the coated steel samples presented OCP values higher than the uncoated sample. For the single- and double-coated steel samples with zirconium-based sol–gel, the potentials increase rapidly, and after 1 h, relatively constant OCP values of −0.060 and −0.123 V are reached, respectively. In the case of the steel coat with the hybrid organic–inorganic film, the OCP increases progressively with time attaining after 25 h potential values greater than the samples coated with zirconium based sol–gel, with a maximum value of 0.008 V for an exposure time of 70 h.

From Fig. 4b, the anodized steel sample reveals an OCP value of −9 mV after 25 h, which is about 300 mV higher than the mechanical polished sample. This potential value does not change for the single-coated sol–gel sample, but it is reduced to some extent for the double-coated sample. In contrast, when the anodized steel sample is coated by the hybrid organic–inorganic film, the OCP increases markedly to about 328 mV, which is approximately 340 more positive than that of the anodized sample. The influence of the different coatings on the differently pretreated steel samples is discussed later with regard to the electrochemical and impedance spectroscopy measurements.

## Electrochemical responses

### *Measurements after an immersion time of 30 min*

Figure 5 shows the *E–I* curves of the differently pretreated coated and uncoated steel samples and Table 1 summarizes the electrochemical parameters calculated from these curves. All the curves show in the anodic direction a passive region of a potential range depending on the

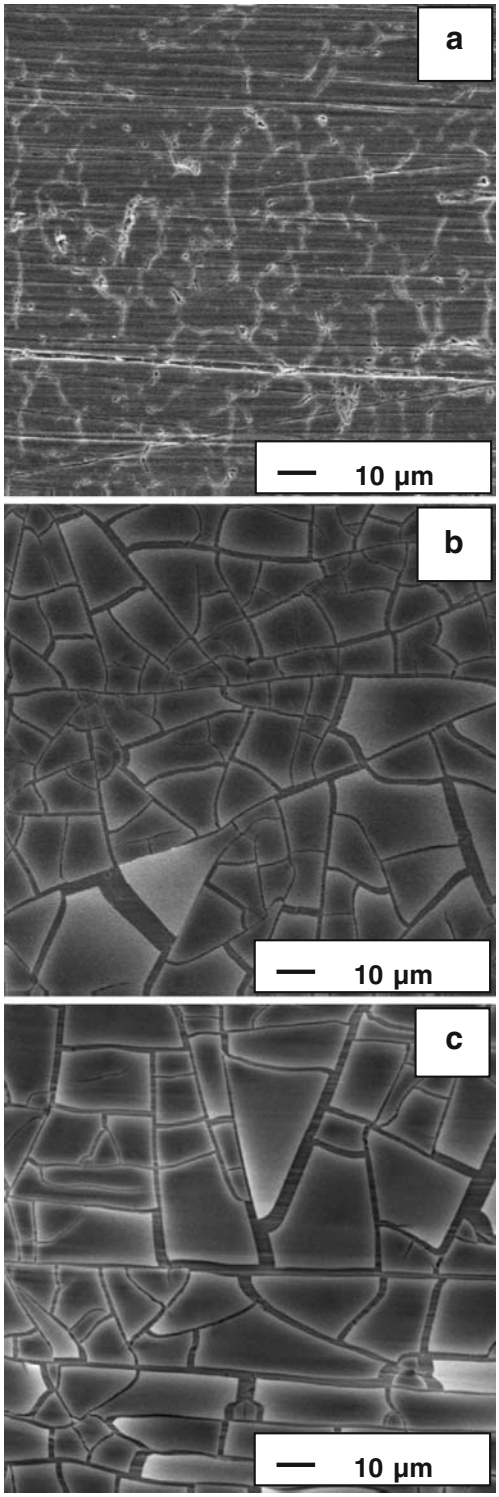


**Fig. 2** Scanning electron micrograph showing the surface morphology of uncoated and coated anodized 316L stainless steel. **a** Uncoated sample, **b** zirconia single-coated sample, **c** zirconia double-coated sample

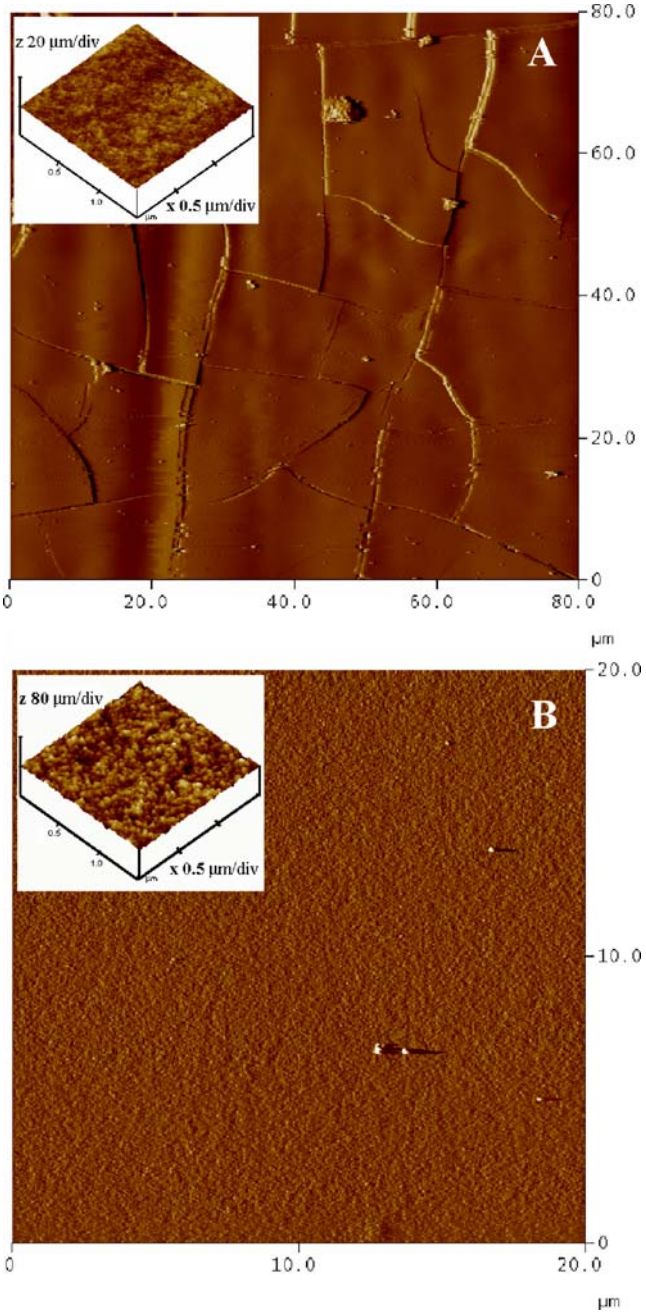


**Fig. 3** Atomic force micrographs showing the surface morphology of differently coated mechanical polished 316L stainless steel. **a** Zirconia single-coated steel surface, **b** hybrid sol–gel-coated steel surface

particular electrode studied. A sudden increase of the current is observed at a higher potential, named $E_b$, possibly associated with the break of the film. Oxygen evolution due to water oxidation was visually observed under these conditions. For some coated samples, the abrupt current increase was followed by a decay of current to the original *I–E* base line, indicating healing of the cracked film region. However, with further anodic polarization, the current starts augmenting again, with

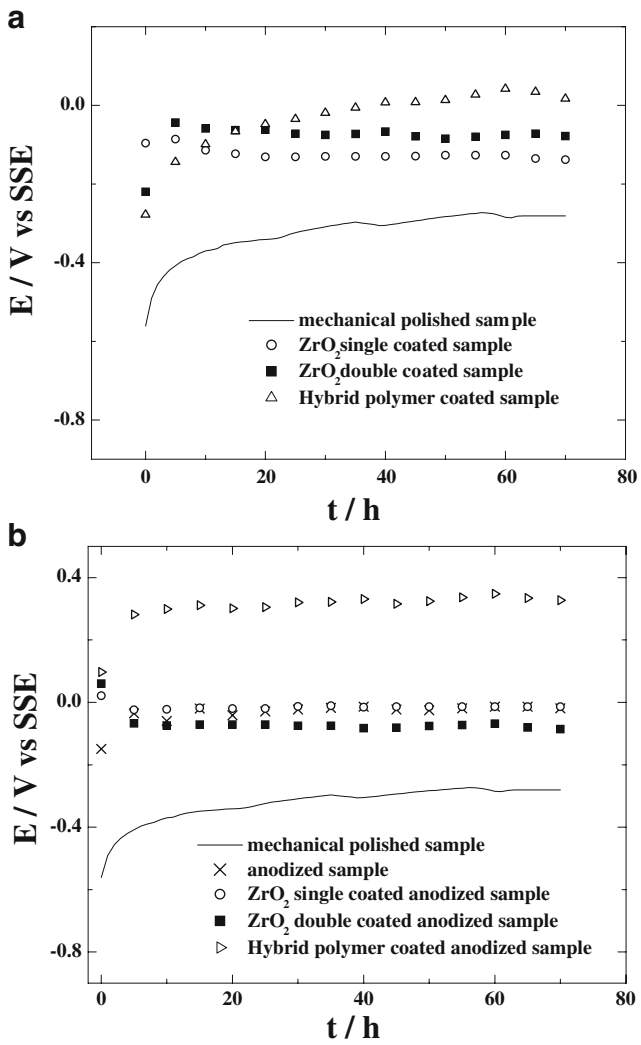


**Fig. 4** Open circuit potential behavior of uncoated and coated 316L stainless steel samples. **a** Mechanical polished pretreated samples, **b** anodized pretreated samples

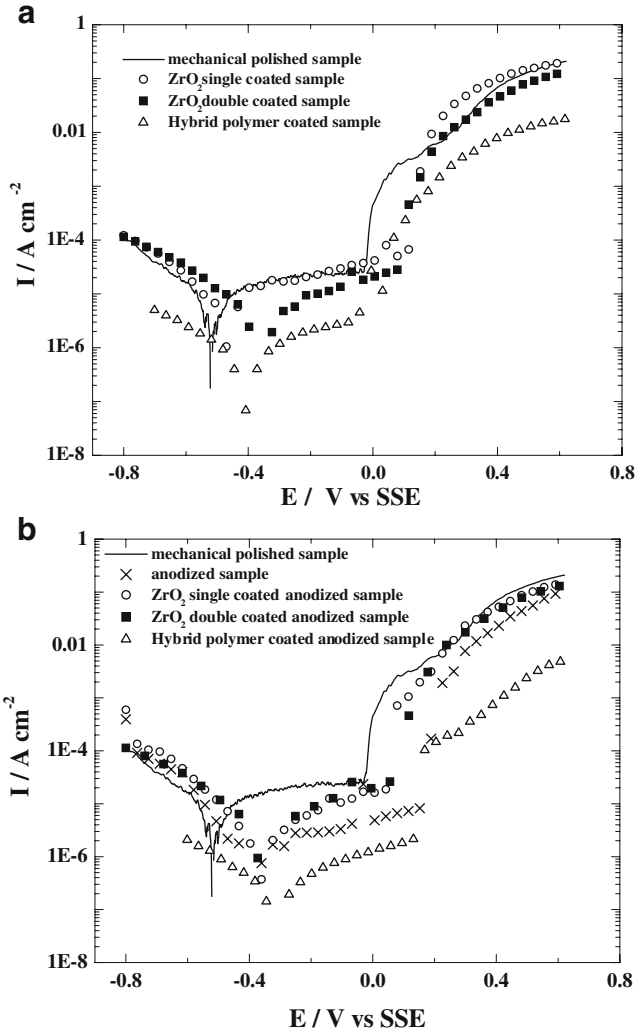


**Fig. 5** Current density–voltage curves of uncoated and coated (**a**) mechanical polished and (**b**) anodized 316L stainless steel samples obtained after an immersion time of 30 min in 0.1 M NaCl

abundant oxygen evolution at the electrode surface, with no recovering of the protective films.

In general, the corrosion potentials calculated from the polarization curve are somewhat different to the OCP values from Fig. 1. However, such differences are expected considering the methodology employed to measure the *E–I* response. The polarization curves were obtained after immersing the steel electrode for 30 min in the electrolyte, which is within the time period where the electrode surface is active.

From comparison of the *E–I* responses in Fig. 5a, the single-coated zirconia sample reveals an $I_{corr}$ relatively similar to that of the uncoated metal substrate, indicating that the overall corrosion process in the initial stage is not affected by the presence of the film. However, the difference ($E_b - E_{corr}$) for the single-coated steel sample is 100 mV greater than that of the uncoated sample, suggesting that for long time of exposure to the electrolyte, the sol–gel film would retard film-cracking events. In Fig. 5a, a second layer of sol–gel coating (double-coated sample) reduces $I_{corr}$ of the uncoated steel sample by a factor of two, implying a higher linked resistance for oxidation of the metal substrate. This correlates well with the SEM micrographs of the coated steel samples, where terrace areas delineated by the coating are larger for the double-coated sample than for the single-coated and the double-coated steel sample. However, the difference ($E_b - E_{corr}$) for the double-coated steel sample is reduced by about 40 mV with respect to that of the uncoated steel sample. Conversely, the presence of the hybrid sol–gel decreases markedly the cathodic and anodic responses resulting in an $I_{corr}$, ten times lower than that of the

uncoated steel sample. This appears to be related to the high uniformity of the film in Figs. 2d and 3b. Although the presence of a thicker zirconia film, or a hybrid polymer film, decreases the corrosion current of stainless steel, the ($E_b - E_{corr}$) difference is not altered with respect to the uncoated sample, the last as a result of a displacement of both, $E_{corr}$ and $E_b$, in the anodic direction.

Figure 5b illustrates the *E–I* responses of the anodized steel surfaces. The uncoated anodized steel sample reveals a lower corrosion current and a higher corrosion potential than that of the mechanical polished steel sample, implying the presence of an anodic film. This film limits mainly oxidation of the metal substrate, since the cathodic current for the mechanical polished and anodized substrate are relatively similar. Further, for the anodized steel sample, the difference ($E_b - E_{corr}$) is about 90 mV more positive than that of the mechanical polished steel samples. This is possibly associated with the composition and morphology of the anodic film limiting incorporation of species from the electrolyte and enhancing passivation of the metal substrate.

In Fig. 5b, the zirconia-coated anodized steel (named single and double) reveals a corrosion potential a little higher than that of the anodized sample but a corrosion current to some extent greater than the anodized steel sample. This may be associated mainly with an increase of the anodic current at potentials higher than the corrosion potential, which also affect its passivity range. The difference ($E_b - E_{corr}$) is reduced in about 180 mV with the presence of the zirconia film. The influence of sol–gel coatings in increasing the corrosion current of the anodized steel substrate could be related to a loss of film adhesion and/or to water uptake from the electrolyte, which enhances blistering and sol–gel film delamination [18–19]. Such processes may be initiated at film cracking regions (Figs. 1 and 2), where incipient lost of adhesion possibly occur, giving rise to an increase of the anodic area and then to an increase in the anodic current. In addition, the rich chromium content (EDX analysis) at film cracked regions above second phases is expected to enhance the cathodic activity and, consequently, film delamination [20–22]. In contrast, the presence of a hybrid sol–gel film decreases strongly the corrosion current, maintaining relatively constant the extension of the passivity region ($E_b - E_{corr}$). This is in good agreement with the high uniformity of the hybrid sol–gel revealed by AFM examinations (Fig. 3a, b). Nevertheless, the protective characteristic of the hybrid sol–gel is not only the result of the film morphology but also the composition of such films is expected to play an important role, since the hydrophobic characteristic conferred by the alkyl chains may change the surface charge and ionic migration throughout the film.

*Measurements after 5 h immersion*

Figure 6 illustrates the polarization curves of the differently pretreated steel samples obtained after an immersion time of 5 h in 0.1 M NaCl, and Table 1 illustrates the corrosion parameters calculated from the *E–I* responses. From Table 1, the corrosion currents for the samples exposed to the electrolyte for 5 h are generally lower than those obtained immediately after immersion. This is more marked for the uncoated than for the coated metal substrates, where a reduction in the corrosion current of about 100 times is revealed. Such a reduction in the corrosion current with immersion time is the expected performance of metals surfaces having active–passive behavior. As shown in Fig. 4, the OCP of the uncoated and coated steel samples is displaced in the anodic direction with immersion time. In the particular case of stainless steel, it has been associated

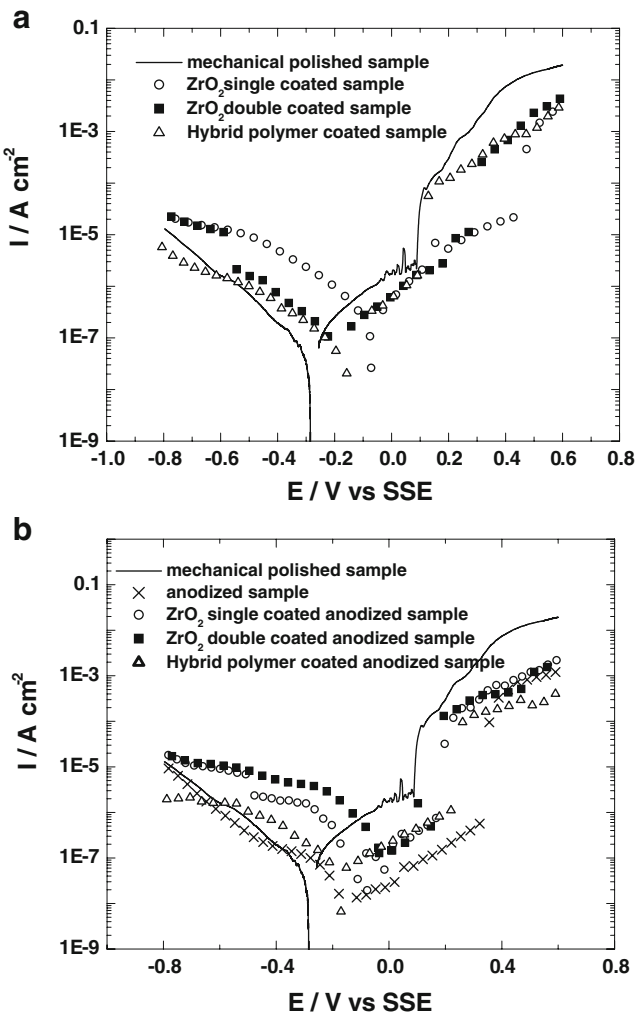


**Fig. 6** Current density–voltage curves of uncoated and coated (**a**) mechanical polished and (**b**) anodized 316L stainless steel samples obtained after 5 h immersion in 0.1 M NaCl

**Table 1** Parameters obtained from data potentiodynamic polarization at 25 °C of uncoated and coated differently pretreated 316 stainless steel samples (Figs. 5 and 6)

| Coating type | Immediately after immersion | | After 5 h immersion | |
|---|---|---|---|---|
| | $E_{corr}$ (V vs. SSE) | $I_{corr}$ (A cm$^{-2}$) | $E_{corr}$ (V vs. SSE) | $I_{corr}$ (A cm$^{-2}$) |
| Mechanically polished samples | | | | |
| Uncoated steel sample | −0.51 | 7.8E−6 | −0.30 | 8.1E−8 |
| $ZrO_2$ single-coated sample | −0.48 | 6.9E−6 | −0.08 | 3.6E−7 |
| $ZrO_2$ double-coated sample | −0.37 | 3.4E−6 | −0.19 | 1.5E−7 |
| Hybrid polymer-coated sample | −0.42 | 7.1E−7 | −0.17 | 6.1E−8 |
| Anodized samples | | | | |
| Uncoated steel sample | −0.41 | 8.3E−7 | −0.15 | 9.1E−9 |
| $ZrO_2$ single-coated sample | −0.37 | 2.7E−6 | −0.08 | 1.1E−7 |
| $ZrO_2$ double-coated sample | −0.36 | 3.9E−6 | −0.01 | 6.3E−7 |
| Hybrid polymer-coated sample | −0.32 | 2.5E−7 | −0.18 | 6.0E−8 |

with metal dissolution and film formation processes proceeding at the metal–electrolyte interface.

From Fig. 6, the zirconia- and hybrid polymer-coated steel samples show cathodic currents greater than the corresponding uncoated samples increasing, consequently, the overall corrosion process as indicated for the $I_{corr}$ values. It is interesting that the *E–I* response of the uncoated anodized sample (Fig. 6b and data in Table 1) readily reveals protection to stainless steel, suggesting that the anodic film formed during anodizing is possibly compact and highly adhered or attached to the metal surface. However, when the anodized substrates are coated by sol–gel coatings, such a protection is reduced considerably, as evident from the augment in the cathodic and anodic currents. The lack of protection is the result of the film system detachment and, consequently, an increase of both the anodic and cathodic areas. The detachment of the film system was evident from SEM examinations, which are not shown here. The mechanism by which the coatings gradually lose adhesion is unknown, owing to the complexity of the metal-film system and numerous variables affecting both, coating-electrolyte and metal-coating interfaces. In addition, synergism among the different variables

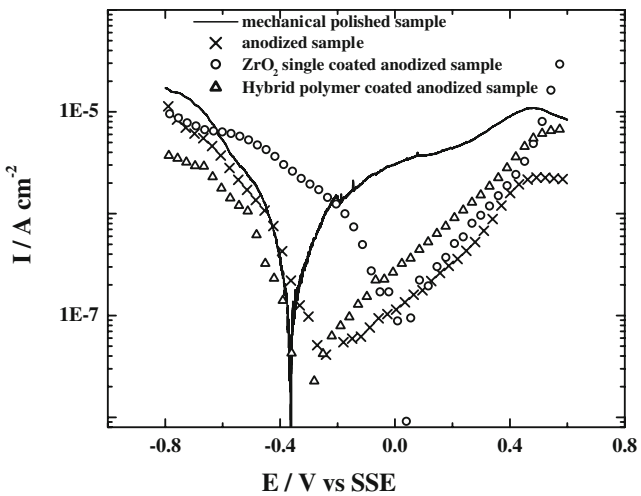


**Fig. 7** Current density–voltage curves of uncoated and coated mechanical polished and anodized 316L stainless steel samples obtained after 5 h immersion in 0.1 M $Na_2SO_4$

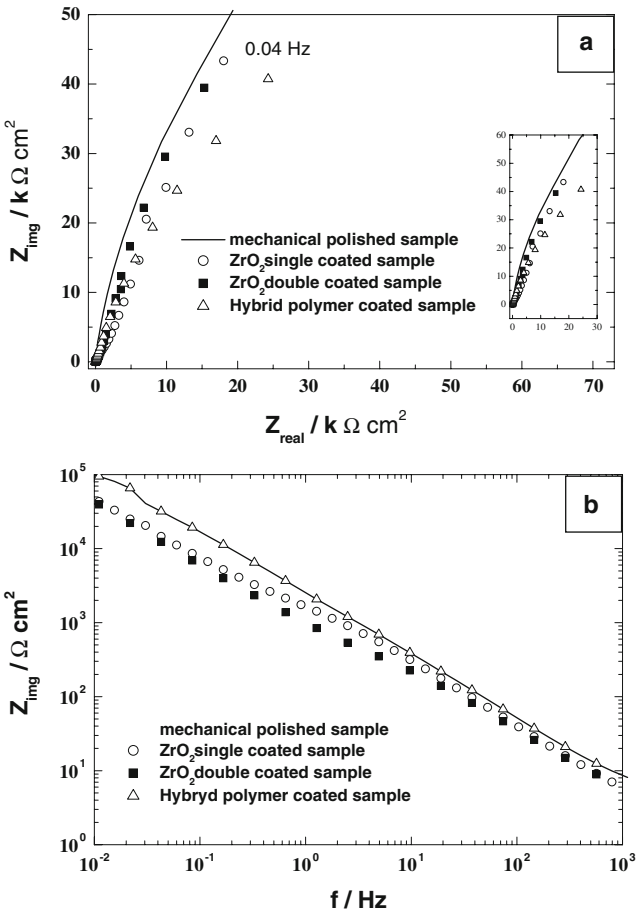


**Fig. 8** AC impedance diagrams of uncoated and coated mechanically polished steel samples obtained after 5 h immersion in 0.1 M NaCl. **a** Nyquist diagram, **b** imaginary part vs. frequency

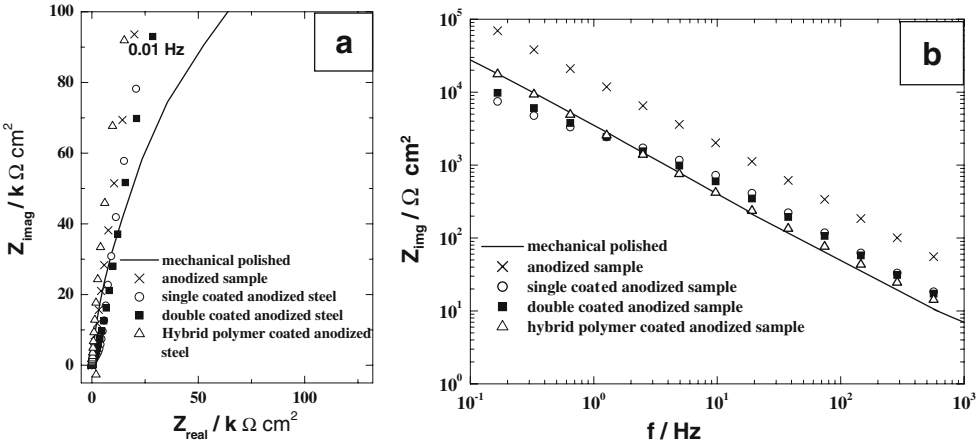


**Fig. 9** AC impedance diagrams of uncoated and coated anodized steel samples obtained after 5 h immersion in 0.1 M NaCl. **a** Nyquist diagram, **b** imaginary part vs. frequency

influencing the stability of such film systems is also expected. However, it seems that the heat treatment to remove the solvent affects the anodic film–sol–gel film interface, play an important role by possibly increasing adhesion of the sol–gel film to the anodic oxide surface, then the sol–gel film shrinkage removes easily the complete coating system. A lose of protection associated with hydration of the anodic film, enhanced by the water uptake from the electrolyte, is though to be insignificant, since the uncoated anodized steel sample shows a high stability even after 5 h of immersion in the electrolyte.

To elucidate if the loss in protection was due to a mechanism involving chloride ions, the electrochemical responses of the differently pretreated stainless steel in 0.1 M sodium sulfate solutions were examined (Fig. 7). When comparing the *E–I* responses in sodium chloride and sodium sulfate solutions (Figs. 6 and 7), the main difference observed is the anodic response in the passivity region, which is evidently altered in the presence of an ion susceptible to induce pitting, such as chloride. However, despite that difference, the general corrosion behaviors of the uncoated and coated steel samples in Fig. 7 are relatively similar to those in a sodium chloride solution (Fig. 6). The increase in the corrosion current is clearly influenced by an increase in the cathodic response implying that the loss of film adhesion proceeds preferentially at film-cracking regions and it is independent of the type of anion involved. Furthermore, the increase in corrosion resistance attributed to the anodic film of stainless steel is more pronounced in the sodium sulfate solution than in the sodium chloride solution. The extrapolation of the corresponding corrosion current density of the mechanical polished and anodized samples (see Figs. 6 and 7) gives the protection efficiency calculated from Eq. 1. This gives a value of 100% of corrosion inhibition in $Na_2SO_4$ and about 60% in NaCl.

$$\frac{I_{\text{corr}}^{\text{polished}} - I_{\text{corr}}^{\text{anodized}}}{I_{\text{corr}}^{\text{polished}}} \times 100 = \text{Eficiency}. \quad (1)$$

*Impedance measurements*

The impedance measurements were performed after 5 h of immersion. A shorter immersion time was difficult to plan due to the evolution of the system (see Fig. 4). In each case under investigation, the impedance diagram appears to be

**Table 2** Parameters obtained from data impedance diagrams (Figs. 8 and 9) of uncoated and coated differently pretreated 316L stainless steel samples, obtained after 5 h immersion in 0.1 M NaCl

| Coating type | *E* (V vs. SSE) | *I* (A cm$^{-2}$) | $\|Z\|_{f=65\ \text{kHz}}$ (Ω cm$^2$) | \|Alpha\| | *Q* (Fcm$^{-2}$ s$^{(\alpha-1)}$) | $C_{\text{dl}}$ (F cm$^{-2}$) |
|---|---|---|---|---|---|---|
| Mechanical polished | | | | | | |
| Uncoated | −0.30 | 8.1E−8 | 24 | 0.90 | 5.E−5 | 18.E−6 |
| $ZrO_2$ single | −0.08 | 3.6E−7 | 22 | 0.79 | 1.6E−4 | 15.E−6 |
| $ZrO_2$ double | −0.19 | 1.5E−7 | 17 | 0.76 | 1.4E−4 | 8.5E−6 |
| Hybrid | −0.17 | 6.1E−8 | 36 | 0.86 | 8.E−5 | 16.E−6 |
| Anodized | | | | | | |
| Uncoated | −0.15 | 9.1E−9 | 26 | 0.87 | 1.4E−5 | 2.5E−6 |
| $ZrO_2$ single | −0.08 | 1.1E−7 | 22 | 0.87 | 3.9E−5 | 8.5E−6 |
| $ZrO_2$ double | −0.01 | 6.3E−7 | 20 | 0.87 | 4.5E−5 | 10.E−6 |
| Hybrid | −0.18 | 6.0E−8 | 19 | 0.8 | 9.E−5 | 7.8E−6 |

more or less the same which corresponds to the beginning of a circle in Nyquist plots (Figs. 8a and 9a). As a first approximation, this behavior can be analyzed by considering a constant phase element (CPE):

$$Z_{\mathrm{CPE}} = \frac{1}{Q(j2\pi f)^{\alpha}}. \quad (2)$$

The frequency range under consideration is limited to 1 kHz in high frequency due to the effect of the current and potential distribution as shown in recent papers [23–24]. The CPE parameters are obtained first by plotting the experimental data as the logarithm of the imaginary part vs. the logarithm of the frequency [25]. The slope of the imaginary part of the impedance on a logarithmic plot is more or less independent of the frequency (Figs. 8b and 9b) and has a value of $-\alpha$. The corresponding values are given in the Table 2.

In a second step, an effective CPE coefficient may be obtained directly from the imaginary part of the impedance as [21]:

$$Q_{\mathrm{eff}} = \sin\left(\frac{\alpha\pi}{2}\right)\frac{-1}{Z_{\mathrm{img}}(f)(2\pi f)^{\alpha}}. \quad (3)$$

From the CPE parameters, it is possible to derive an approximate value of the capacitance by applying the Brug's formula [26]. All values obtained are of the order of 10 μF/cm$^2$, which can correspond to a double layer capacitance. Only the uncoated anodized sample presents clearly different impedance (Fig. 9b) and the corresponding capacitance is about 2 μF/cm$^2$. This value is in agreement with a capacitance of an oxide film with a thickness of a few nanometers [26–28].

All the coatings have no effect after 5 h of immersion for mechanical polished samples which correspond to films completely detached from the substrate. For the anodized sample, after 5 h of immersion, the films are also completely detached but these coating have modified the sample by modifying or destroying the oxide layer.

## Conclusions

1. The zirconia sol–gel polymer produces nonhomogeneous coatings on 316L stainless steel, either mechanically polished or anodized. The inorganic polymer covers preferentially grains of the metal substrate, leaving film-free grain boundary regions
2. The grade of protection given by the coatings depended on the immersion time in 0.1 M NaCl. Thus, from potentiodynamic experiments after short immersion time, protection is evident. However, with increasing the exposure time to 5 h, the corresponding films are partially detached and the corrosion currents are greater than those of the uncoated steel sample
3. The potentiodynamic and impedance measurements revealed the convenience of anodizing the 316L stainless steel to increase its corrosion resistant in 0.1 M NaCl. The presence of the anodic film strongly reduced the corrosion current of the stainless steel and also increases the difference between the potential where the film presumably suffers cracking, named $E_b$, and the corrosion potential, $E_c$. However, anodizing as a pretreatment to increase adhesion of the sol–gel and the hybrid polymer films is not appropriate.

**Acknowledgements** The authors are grateful to Fondecyt (Grant: 1060050), CONICYT-Programa Bicentenario in Science and Technology and to DICYT (USACH) for financial support. H. Torres is grateful to the Alpha program, scholarship (RICICOP-II).

## References

1. Jones DA (1996) Principles and prevention of corrosion, 2nd edn. Prentice-Hall, New Jersey
2. Shreir LL, Jarman RA, Burstein GT (1994) In: Shreir LL, Burstein GT (eds) Corrosion. Butterworth-Heinemann, Oxford
3. Buchheit R (1994) J Electrochem Soc 142:3994 doi:10.1149/1.2048447
4. Marcin A, Malik MA, Włodarczyk R, Kulesza PJ, Bala H, Miecznikowski K (2005) Corros Sci 47:771 doi:10.1016/j.corsci.2004.07.022
5. Kulesza PJ, Miecznikowski K, Malik MA, Gałkowski M, Chojak M, Caban K et al (2001) Electrochim Acta 46:4065 doi:10.1016/S0013-4686(01)00687-9
6. Marcin A, Malik MA, Kulesza PJ, Wlodarczyk R, Wittstock G, Szargan R et al (2005) J Solid State Electrochem 9:403 doi:10.1007/s10008-005-0654-x
7. Galkowski M, Kulesza PJ, Miecznikowski K, Chojak M, Bala H (2004) J Solid State Electrochem 8:430 doi:10.1007/s10008-003-0473-x
8. Budiansky ND, Hudson JL, Scullyb JR (2004) J Electrochem Soc 151:B233–B243 doi:10.1149/1.1666168
9. Guglielmi M (1994) J Sol–Gel Sci Technol 78:177
10. Vasconcelos DCL, Carvalho JN, Mantel M, Vasconcelos WL (2000) J Noncryst Solids 273:135 doi:10.1016/S0022-3093(00)00155-1
11. Simoes M, Assis OBG, Avaca LA (2000) J Noncryst Solids 273:159 doi:10.1016/S0022-3093(00)00161-7
12. Messaddeq SH, Pulcinelli SH, Santilli CV, Guastaldi AC, Messaddeq Y (1999) J Noncryst Solids 247:164 doi:10.1016/S0022-3093(99)00058-7
13. Checmanowski J, Gluszek J, Masalski J (2003) Mater Sci 21:387
14. Brinker CJ, Scherer GW (1990) Sol–gel science. The physics and chemistry of sol–gel processing. Academic, San Diego
15. Chou TP, Chandrasekaran C, Limmer S, Nguyen C, Cao GZ (2002) J Mater Sci Lett 21:251 doi:10.1023/A:1014733413682
16. Park JS, Mackencie JD (1995) J Am Ceram Soc 78:2669 doi:10.1111/j.1151-2916.1995.tb08038.x

17. Metroke TL, Parkhill RL, Knobbe ET (2001) Prog Org Coat 41:233 doi:10.1016/S0300-9440(01)00134-5
18. Jackson CL, Bauer BJ, Nakatani AI, Barnes JD (1996) Chem Mater 8:72
19. Martin JW, Embree E, Tsao W (1990) J Coat Tech 62:25
20. Nguyen T, Bentz D, Byrd E (1995) J Coat Tech 67:37
21. van der Meer-Lerk LA, Heertjes PM (1975) JOCCA 58:79
22. Pommersheim JM, Nguyen T (1998) In: Bierwagen GP (ed) Proceedings of the American Chemical Society symposium series No 689—organic coating for corrosion control, chap 11. American Chemical Society, Washington DC, pp 137–150
23. Pebere N, Picand TH, Duprat M, Dabosi F (1989) Corros SC 129:1073 doi:10.1016/0010-938X(89)90045-0
24. Huang VMW, Vivier V, Orazem ME, Pébère N, Tribollet B (2007) J Electrochem Soc 154:C81–C88 doi:10.1149/1.2398882
25. Huang VMW, Vivier V, Frateur I, Orazem ME, Tribollet B (2007) J Electrochem Soc 154:C89–C98 doi:10.1149/1.2398889
26. Orazem ME, Pébère N, Tribollet B (2006) J Electrochem Soc 153: B129–B136 doi:10.1149/1.2168377
27. Brugg GJ, Van den Eeden ALG, Sluyters-Rehbach M, Sluyters JH (1984) J Electroanal Chem 176:275 doi:10.1016/S0022-0728(84)80324-1
28. Carnot A, Frateur I, Zanna S, Tribollet B, Dubois-Brugger I, Marcus P (2003) Corros Sci 45:2513 doi:10.1016/S0010-938X(03)00076-3